# Dynamics of the C 1$s \rightarrow \pi^*$ excitation and decay in $CO_2$ probed by vibrationally and angularly resolved Auger spectroscopy

E. Antonsson,[1,2] M. Patanen,[1] C. Nicolas,[1] S. Benkoula,[1] J. J. Neville,[1,3] V. L. Sukhorukov,[4,5] J. D. Bozek,[1] Ph. V. Demekhin,[5,*] and C. Miron[1,6,†]

[1]*Synchrotron SOLEIL, L'Orme des Merisiers, Saint-Aubin, BP 48, 91192 Gif-sur Yvette Cedex, France*

[2]*Physical Chemistry, Freie Universität Berlin, Takustrasse 3, 14195 Berlin, Germany*

[3]*Department of Chemistry, University of New Brunswick, Fredericton, New Brunswick, Canada E3B 5A3*

[4]*Research Institute of Physics, Southern Federal University, Stachki Avenue 194, 344090 Rostov-on-Don, Russia*

[5]*Institut für Physik und CINSaT, Universität Kassel, Heinrich-Plett-Strasse 40, 34132 Kassel, Germany*

[6]*Extreme Light Infrastructure-Nuclear Physics (ELI-NP), "Horia Hulubei" National Institute for Physics and Nuclear Engineering, 30 Reactorului Street, RO-077125 Măgurele, Judetul Ilfov, Romania*

(Received 3 September 2015; published 12 October 2015)

Participator resonant Auger decay spectra populating the $X$, $A$, $B$, and $C$ states of $CO_2^+$ are recorded with angular and vibrational resolution for selected photon energies in the vicinity of the C 1$s \rightarrow \pi^*$ resonance of $CO_2$ using a narrow photon bandwidth and a high-resolution electron spectrometer. The measured electron spectra and the corresponding angular distribution parameters exhibit significant changes as functions of the photon energy across the resonance and with respect to the vibrational sublevels of a final ionic state. The measured spectra are interpreted by *ab initio* electronic structure and nuclear dynamics calculations which attribute observed variations to the effects of lifetime vibrational interference and of electronic state interference between the direct ionization amplitude and the resonant amplitudes for the excitation and decay of two overlapping resonant states of different symmetry. The present results provide deeper insight into the femtosecond relaxation dynamics of the core-excited $CO_2$, which is not achievable with lower resolution, angle-averaged measurements.

DOI: 10.1103/PhysRevA.92.042506 PACS number(s): 33.20.−t, 33.80.−b, 32.80.Hd

## I. INTRODUCTION

In order to study resonant photoemission following core excitation of molecules in the Auger-Raman regime [1,2], the bandwidth of the exciting radiation should be smaller than the natural lifetime width of the excited vibronic resonances. This allows one to selectively excite individual vibronic states and to study the interplay between nuclear dynamics in core-excited molecular states and the electron dynamics, governed by the Auger decay of these states, taking place on similar femtosecond time scales. Since the broadening of electron lines under the Auger-Raman conditions is not constrained by the natural lifetime width of the core-excited states, vibrationally resolved studies where the different vibrational sublevels of the final molecular ionic states can be individually resolved become feasible.

Increasing excitation selectivity in the spectroscopy of dilute species is always a trade-off between the degree of monochromaticity and the photon flux of the exciting radiation. Advances in the generation of soft x rays at modern beamlines of the third-generation synchrotron light sources, offering ever higher photon fluxes and narrower bandwidth, have lead to an increasing number of important results in materials science, such as the possibility to study structure and dynamics of highly excited molecular states in the Auger-Raman regime [3,4]. It is, therefore, not a surprise that a number of vibrationally resolved resonant Auger (RA) decay studies have already been performed on diatomics, such as $N_2$ [5–9], CO [9], $O_2$ [9,10], NO [11–14], and KF [15], and on small polyatomics $C_2H_4$ [16], $C_2H_4BrCl$ [17], $CH_4$ [18,19], $CH_3Cl$ [20], $CO_2$ [21], $N_2O$ [22,23], and OCS [24], where the diversity of relevant nuclear degrees of freedom increases the complexity of the process.

Complementary information on the femtosecond-time-scale competition between nuclear and electron dynamics in the core-excited molecular states can be obtained by means of the electron-ion coincidence spectroscopy [25,26], and the vibrationally and angularly resolved electron spectroscopy [4]. Being very sensitive to the interplay between the outgoing partial electron continuum waves [27], angular distributions of emitted electrons provide access to specific interference effects [28–33], which cannot be observed in the total decay spectra. These advantages of the angular resolution have already been utilized to investigate relaxation dynamics of core-excited states in diatomics, such as CO [28,29,34,35], NO [31,32,36], and $O_2$ [33], and even in polyatomics molecules, such as $C_2H_2$ [30], $CO_2$ [37], $H_2O$ [38], and $N_2O$ [39]. In the present work, we investigate the RA decay of the triatomic $CO_2$ after core excitation of the central carbon atom.

In the neutral ground state, $CO_2$ has linear geometry and its electronic configuration is $1\sigma_g^2 1\sigma_u^2 2\sigma_g^2 3\sigma_g^2 2\sigma_u^2 4\sigma_g^2 3\sigma_u^2 1\pi_u^4 1\pi_g^4 (^1\Sigma^+)$. Here the $1\sigma_{g,u}$ orbitals originate from the 1$s$ electrons of oxygen and the $2\sigma_g$ orbital corresponds to the 1$s$ electrons of the centrally located carbon atom. For $CO_2$ in the linear ($D_{\infty h}$) geometry, the $1s^{-1}\pi^*(^1\Pi_u)$ core-excited state is doubly-degenerate. In the bent ($C_{2v}$) geometry, the degeneracy is lifted, yielding the two Renner-Teller split but still strongly overlapping core-excited states of the $^1A_1$ and $^1B_1$ symmetries [21,40,41]. A similar Renner-Teller effect is also present in other simple triatomic molecules, such as $N_2O$, OCS, and $CS_2$ [22,24,41–43]. The statically bent $^1A_1$ state is lower in energy than the linear $^1B_1$ one. As a consequence,

*demekhin@physik.uni-kassel.de

†catalin.miron@synchrotron-soleil.fr

 

excitations on the lower-energy side of the broad C $1s \rightarrow \pi^*$ resonance preferentially populate the bent $^1A_1$ core-excited state. Contrary to that, excitations in the middle and on the high-energy side create a coherent superposition of the linear $^1B_1$ and bent $^1A_1$ states [21,40,41].

In the present work we perform a vibrationally and angularly resolved study of the RA decay following C $1s \rightarrow \pi^*$ excitations in $CO_2$. The present work goes significantly beyond the previous vibrationally and angularly resolved study of $CO_2$ [37]. There the RA electron spectra were recorded for the $A$ and $B$ final states only at the excitation maximum with the photon bandwidth of about 30 meV. Here we investigate $X$, $A$, $B$, and $C$ participator channels at different excitation energies across the C $1s \rightarrow \pi^*$ resonances with a considerably smaller photon bandwidth. This allows us to selectively trigger different electronic and nuclear wave packets in core-excited states of different symmetry. The paper is organized as follows. The present experimental technique and theoretical framework are outlined in Secs. II and III, respectively. The measured and computed vibrationally and angularly resolved excitation and decay spectra of $C^*O_2$ are compared and discussed in Sec. IV. We conclude in Sec. V with a brief summary.

## II. EXPERIMENT

The experiments were performed at the PLEIADES beamline at the SOLEIL synchrotron radiation facility that is dedicated to ultrahigh-resolution soft x-ray studies of dilute samples ranging in size from gaseous atoms [44] and molecules [7,45] to proteins [46], van der Waals clusters [47] and freestanding nanoparticles [48,49].

The $CO_2$ gas was purchased from Sigma-Aldrich and had a stated purity of 99.998%. The sample was contained in a gas cell equipped with electrodes for plasma potential correction. The sample pressure in the spectrometer chamber was typically $5\times10^{-6}$ mbar and estimated to be at least 2 orders of magnitude higher in the gas cell. A 2400 l/mm grating with variable groove depth was used to monochromatize the x rays. A photon bandwidth of 13 meV was chosen for the resonant photoemission measurements near the C $1s$ edge. The photon energy was calibrated using the C $1s \rightarrow 3s$ transition energy value of $292.74 \pm 0.02$ eV [41]. The RA electron spectra were recorded at different photon energies on and off resonance (see Sec. IV A). In addition, the total ion yield was recorded across the whole C $1s \rightarrow \pi^*$ resonance in steps of 25 meV using a somewhat larger photon bandwidth of 50 meV.

The electron spectra were recorded using a VG Scienta R4000 hemispherical electron analyzer. A curved entrance slit of 0.2 mm and a pass energy of 20 eV were used for the electron spectrometer. These settings resulted in a spectrometer resolution of 10 meV. Translational Doppler broadening due to the thermal motion of the sample molecules at room temperature, estimated to 31 meV [50], is probably the largest contribution to line broadening in the experiments, but rotational Doppler broadening is also expected to occur with a comparable magnitude [51,52]. The electron energy was calibrated using the average binding energy 13.787 eV of the $CO_2^+(X)$ ground-state doublet [53]. The spectra were normalized with respect to photon flux, sample pressure, and acquisition time to ensure a reliable determination of the angular anisotropy parameters.

## III. THEORY

In order to study excitation and RA decay of the $CO_2$ molecule, we applied the theoretical approach used in our previous angularly resolved studies of the core-excited CO [28,29], NO [31,32], and $N_2O$ [39] molecules. Below we outline only its essential points. The working equations required to compute photoionization transition amplitudes in the vicinity of the core-excitation and the angularly resolved RA electron spectra of a polyatomic molecule can be found in Ref. [39] [see Eqs. (7)–(10) therein].

The three-dimensional nuclear dynamics of the symmetric and asymmetric stretching and of the bending modes in $CO_2$ were computed by the multiconfiguration time-dependent Hartree (MCTDH) method [54,55]. The required potential energy surfaces (PESs) were obtained by the full valence complete active space multiconfiguration self-consistent field calculations with subsequent multireference configuration interaction approach, as described in detail in [56,57]. Similar to the previous studies of the core-excited $N_2$, CO, NO, and $N_2O$ molecules [6,14,28,39], the resonant states were computed in the equivalent core "$Z+1$" approximation (see also Sec. IV A).

Calculations of the electronic part were carried out by the single center (SC) method [58–61], which provides accurate partial electron continuum waves in molecules. Detailed description of the stationary SC method for diatomics can be found in Refs. [58,59]. Its extension to polyatomics and the time-dependent formulation of the method are given in Refs. [60] and [61], respectively. In the calculations of the photoionization matrix elements, (i) the lifetime vibrational interference (LVI [62]), (ii) the electronic state interference (ESI [63]) between the direct and the resonant amplitudes for the population of the final ionic states, and (iii) the monopole relaxation of the molecular orbitals in the field of the core-vacancy were accounted for, as described in the previous studies of core-excited molecules [28,29,31,32,39].

At the instant of the core-excitation the $CO_2$ molecule has linear geometry, and, immediately after, the RA decay and underlying nuclear dynamics start to compete with each other. The triple-ion-coincidence measurements of Ref. [40] have demonstrated that dissociation geometry after electronic decay of the $^1B_1$ excited state is mainly linear. On the contrary, being excited to the $^1A_1$ state, the molecule starts to bend rapidly. The lifetime of the C $1s$ hole of 6.9 fs (corresponds to the line broadening of 95 meV [64]) is only three times smaller than the half of the bending period $\pi/\omega_2 = 20.3$ fs in the $^1A_1$ state (estimated by using $\omega_2 = 102$ meV [21]). As a result, the bending geometry distribution during the RA decay of the individually excited $^1A_1$ state has a long tail which extends to about 100° bending angle, with the main peak at about 155° [40].

The present calculations of the electronic transition amplitudes for the excitation of the $^1A_1$ and $^1B_1$ states, direct ionization into the $X$, $A$, $B$, and $C$ states of $CO_2^+$, and RA decay of the $^1B_1$ state were performed in the linear geometry at the equilibrium internuclear geometry of the ground electronic state of $CO_2$. As discussed above, it is

important to reflect bending geometry of a molecule when computing the electronic transition matrix elements for RA decay of the $^1A_1$ state. Those amplitudes were computed at several bending angles between 100° and 180°. It was found that agreement between the present theoretical and experimental angularly resolved spectra change insignificantly for different bent geometries of the $^1A_1$ state, but considerably deteriorates if the linear geometry, 180°, is considered instead. In order to obtain the final computational results shown in Sec. IV, we used the amplitudes for the RA decay of the $^1A_1$ state obtained in the maximum of the bending geometry distribution at the bending angle of 155° [40].

## IV. RESULTS AND DISCUSSION

### A. The C 1$s \rightarrow \pi^*$ excitation

The total ion yield spectrum recorded in the vicinity of the C 1$s \rightarrow \pi^*$ transition in $CO_2$ is shown in Fig. 1 by circles. In contrast to what was found below the O 1$s$ edge of $CO_2$, where the O 1$s \rightarrow \pi^*$ resonance overlaps with a transition to a Rydberg state [65], the C 1$s \rightarrow \pi^*$ excitation is well separated from other spectral features. Transitions to Rydberg-type states below the C 1$s$ edge of $CO_2$ occur only 2 eV above the maximum of the C 1$s \rightarrow \pi^*$ peak and are neatly separated from it [43]. Such transitions thus do not contribute to the Auger decay spectra measured here, which can be assumed to solely reflect the decay of the C 1$s \rightarrow \pi^*$ resonances. The broad (about 0.7 eV full width at half maximum) resonance corresponds to unresolved transitions to different vibrational levels of the overlapping $^1A_1$ and $^1B_1$ electronic states [21].

The presently computed total C 1$s \rightarrow \pi^*$ excitation spectrum (solid curve in Fig. 1) was obtained as the sum of equal contributions of the two partial spectra for the excitation of $^1A_1$ and $^1B_1$ electronic states (broken curves). The latter were obtained by the following procedure. It is known that the equivalent core "$Z+1$" approximation is slightly inaccurate [66]. In the first approximation, this inaccuracy can be corrected by applying a slight shift to the distances between the core-excited atom and its neighbors [6,14,28]. In order to model PESs of the $^1A_1$ and $^1B_1$ states of $C^*O_2$, we applied two different shifts $\Delta r_{NO}$ of the internuclear distance $r_{NO}$ to the presently computed PESs of the $NO_2(^2A_1)$ and $NO_2(^2B_1)$ states and used them as free parameters ($NO_2$ is the "$Z+1$" analog for the core-excited $C^*O_2$).

In order to calibrate the vertical excitation energy, we used the procedure suggested in the previous attempt to model the C 1$s \rightarrow \pi^*$ excitation spectrum of $CO_2$ [21] (see Sec. III F and Fig. 7 there). In particular, we assign the slight variations of the total ion yield, seen on the top of the broad hump (open circles in Fig. 1), to the symmetric stretching vibrational progression $\nu_1$ of the linear state $^1B_1$. The present assignment of the $^1B_1(\nu_1)$ progression (indicated at the bottom of Fig. 1) coincides with that suggested in Ref. [21]. The energy fit places the $\nu_1 = 0$ level of the $^1B_1$ state at 290.61 eV, which is close to the value of 290.56 eV from Ref. [21]. The PES of the $NO_2(^2B_1)$ state was, thus, shifted vertically to yield $E(000) =$ 290.61 eV, and the same vertical energy shift was applied to the computed PES of the $NO_2(^2A_1)$ state.

The two $\Delta r_{NO}$ shifts were obtained by the best fit of the computed total excitation spectrum and the measured total ion yield in Fig. 1. During the fit, we also took care that the shifted PESs of the core-excited states provide reasonable RA electron intensity distribution (see Fig. 2). The present fitting yielded $\Delta r_{NO}(A_1) = 0.040$ Å and $\Delta r_{NO}(B_1) = 0.015$ Å, which results in $r_e(A_1) = 1.246$ Å and $r_e(B_1) = 1.221$ Å. For the $^1B_1$ state,

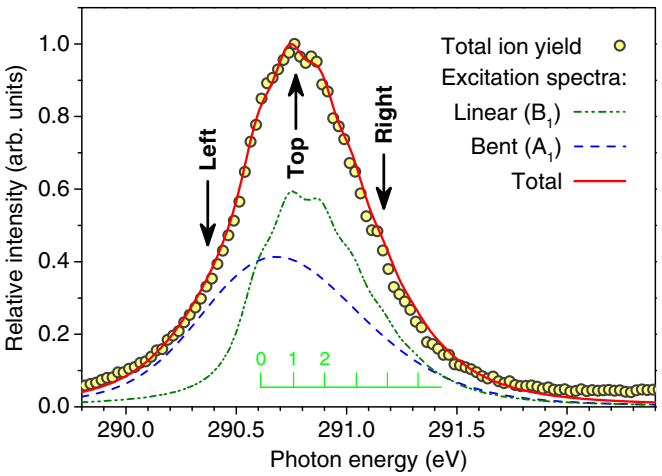


FIG. 1. (Color online) Circles mark the total ion yield spectrum recorded in the vicinity of the C 1$s \rightarrow \pi^*$ resonances of $CO_2$. The vertical arrows mark the energies selected to measure the on-resonance RA electron spectra shown in Figs. 2 and 3. Lines indicate total and partial C 1$s \rightarrow \pi^*$ excitation spectra obtained by the three-dimensional nuclear dynamics calculations. The energies of the $\nu_1$ symmetric vibrational mode of the linear $B_1$ state are also indicated. The total experimental and theoretical spectra are normalized at their maxima. For further details, see Sec. IV A.

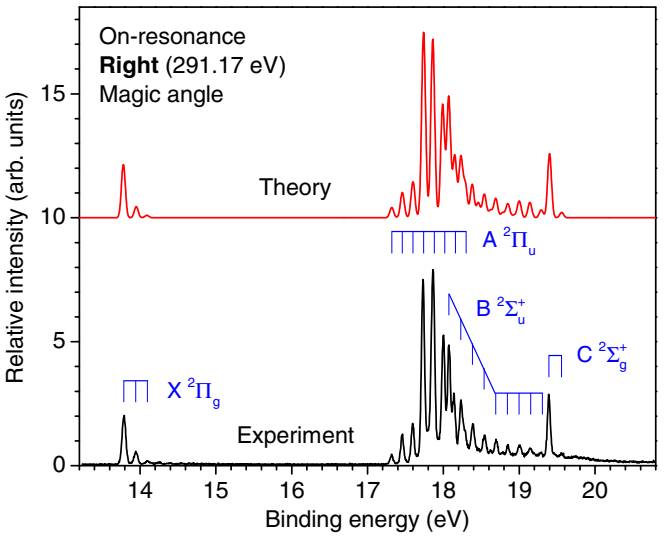


FIG. 2. (Color online) Overview of the participator RA electron spectra of the C 1$s \rightarrow \pi^*$ resonances excited at the photon energy of 291.17 eV (0.4 eV above the maximum, corresponds to the vertical arrow labeled "Right" in Fig. 1). The experimental magic-angle-recorded spectrum is shown at the bottom of the figure. The vertical bars indicate vibrational progressions of the symmetric stretching mode for each of the final electronic states of $CO_2^+$. The computed spectrum is shown in the upper part of the figure. In order to facilitate comparison, experimental binding energy of the ground vibrational level (000) of each final ionic state was used in the calculations.

the presently obtained intensity distribution in the excitation spectrum is very similar to that from Ref. [21] (cf., dash-dotted curve in Fig. 1 here and open squares in Fig. 7 of this reference). In Ref. [21], the symmetric stretching mode $^1A_1(\nu_1)$ was frozen, and a broad intensity distribution was attributed to the coupling of the electronic and nuclear motion angular momenta in the $^1A_1$ state. Here we neglect the angular momenta coupling and interpreted the broad intensity distribution (dashed curve in Fig. 1) in terms of the population of higher symmetric stretching $\nu_1$ and bending $\nu_2$ levels of the $^1A_1$ state.

### B. Participator RA electron spectra

The RA decay spectra of the C $1s \rightarrow \pi^*$ excitation were recorded at three photon energies, i.e., at 290.37, 290.77, and 291.17 eV (marked by vertical arrows in Fig. 1). According to this figure, the photon energy labeled "Left" corresponds to the excitation of the $^1A_1$ bent state, whereas excitations at the photon energies labeled "Top" and "Right" prepare coherent superpositions of the $^1A_1$ bent and the $^1B_1$ linear states. Figure 2 shows an overview of the RA decay spectrum excited at the photon energy of 291.17 eV, which is 0.4 eV higher than the maximum of the C $1s \rightarrow \pi^*$ resonance. It depicts the angle-averaged (equal to the magic-angle-recorded) spectrum, which was obtained as a weighted sum of the two angularly resolved spectra recorded at 0° and 90° relative to the polarization axis of the soft x-ray photons, by using the conventional formula $I_{MA} = (I_{0^\circ} + 2I_{90^\circ})/3$.

Our experimental spectrum (bottom of Fig. 2) is found to be similar to the previously reported, lower resolution spectra [21,67]. The studied binding energy range of 13.5–20.5 eV encompasses the four lowest electronic states of the $CO_2^+$ ion. Vibrational levels of the symmetric stretching mode of the $X$, $A$, $B$, and $C$ states of $CO_2^+$ are marked in the figure with vertical bars. These final electronic states are populated via the so-called participator Auger decay, in which the excited electron takes part in the decay, leaving behind the single valence-hole final states of the ion. The corresponding RA electron spectrum, computed using the PESs of the core-excited states obtained in this study (see discussion in Sec. IV A), is depicted in the upper part of Fig. 2 for comparison. The figure illustrates a very good overall agreement between the computed and the measured RA electron spectrum of $C^*O_2$.

The angularly resolved RA electron spectra recorded along the profile of the C $1s \rightarrow \pi^*$ resonance are collected in Figs. 3(b)–3(d). The spectra were measured for the two electron emission directions, perpendicular (90°) and parallel (0°) to the polarization vector of the x-ray photons. The $X$, $A$, $B$, and $C$ states of $CO_2^+$ populated by the participator RA decay can also be accessed directly via the nonresonant photoionization of the valence shells of $CO_2$. In spite of the high photon energy, the direct ionization channel is non-negligible, and it induces interesting ESI effects [8,28–33,39]. For comparison, the off-resonance photoelectron spectra are also shown in Fig. 3(a). Those spectra were recorded at the photon energy of 285 eV (5.77 eV below the resonance maximum), and they correspond to photoelectrons emitted by the direct ionization of the valence shells of the molecule.

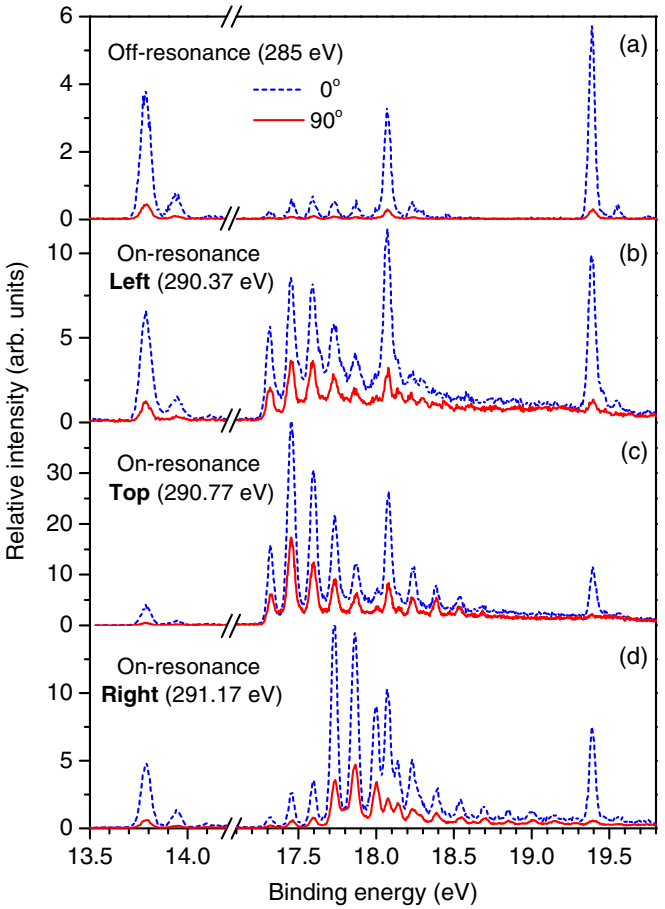


FIG. 3. (Color online) Vibrationally and angularly resolved RA electron spectra after excitation along the C $1s \rightarrow \pi^*$ transition in $CO_2$ for electrons detected parallel (broken curves) and perpendicular (solid curves) to the polarization vector of the exciting photons. (a) Off-resonance excitation at 285 eV (energy detuning is −5.77 eV). (b) On-resonance excitation at 290.37 eV (Left, 0.4 eV below the maximum). (c) On-resonance excitation at 290.77 eV (Top, no detuning). (d) On-resonance excitation at 291.17 eV (Right, 0.4 eV above the maximum). Note the energy-axis break in between 14.2 and 17.1 eV.

From Fig. 3 it is evident that the $X\ ^2\Pi_g(\nu_1)$ RA electron peaks do not show significant resonant enhancement. This ionic state corresponds to the removal of an electron from the $1\pi_g$ molecular orbital, which is mostly composed of oxygen atomic orbitals with a small contribution from carbon orbitals in a bent geometry. This results in a very small overlap between the $1\pi_g$ electron and the C $1s$ core-hole, which is localized on the central carbon, and, as a result, in a very low partial RA decay rate for the $X$ state. This argumentation is consistent with the observations of Ref. [37], which reports significant resonant enhancement of the $X\ ^2\Pi_g(\nu_1)$ RA electron peaks across the O $1s \rightarrow \pi^*$ excitation, where $1\pi_g$ electron has large overlap with the O $1s$ hole.

As discussed in Sec. III, excitation of the bent $^1A_1$ electronic state results in the population of excited levels of the bending mode. During the RA decay, this population is transferred to the final ionic states, where a significant excitation of the bending motion can also be expected. This

results in a manifold of symmetric stretching vibrational progressions separated by the smaller energy difference of the bending quanta, which leads to a lower "peak-to-valley" contrast in the decay spectra. Figure 3(b), which corresponds to the excitation on the low-energy side of the C 1$s \rightarrow \pi^*$ resonance, supports this argumentation. This is especially apparent in the binding energy range of 18.3–19.3 eV, where the $B\,^2\Sigma_u^+(\nu_1)$ vibrational progression (clearly seen in Fig. 2) is washed out and manifests itself in Fig. 3(b) as a smooth background. In addition, a smooth hump is formed around the binding energy of 18 eV [67,68] due to complex avoided crossings along the bending coordinate $\nu_2$ [69,70].

When the photon energy is increased along the C 1$s \rightarrow \pi^*$ resonance, the linear $^1B_1$ core-excited state starts to play an increasing role, and an enhancement of the population of the symmetric stretching mode $\nu_1$ of the final RA decay states can be expected. Indeed, from Fig. 3(c) one can see longer overlapping $A\,^2\Pi_u^+(\nu_1)$ and $B\,^2\Sigma_u^+(\nu_1)$ vibrational progressions which extend up to the binding energy of about 18.7 eV. For higher excitation energies [Fig. 3(d)], those progressions are even more pronounced, and the latter one can be followed up to about 19.3 eV, where it starts to overlap with the $C\,^2\Sigma_g^+$ band.

While the vibrational envelope in the off-resonance direct ionization [Fig. 3(a)] is determined by the Franck-Condon overlap of the neutral ground and final ionic states, the vibrational envelope in the resonant case is determined by the overlap of the vibrational wave functions of the final ionic and intermediate core-excited states. Thus, populating different intermediate states causes significant changes in the RA electron intensity distribution. Such strong changes are seen when comparing the vibrational envelopes of the $A\,^2\Pi_u$ and $B\,^2\Sigma_u^+$ bands in Figs. 3(b)–3(d) going from negative to positive detuning of the photon energy. The RA decay spectra in Fig. 3 yield valuable information about the nuclear dynamics in the core-excited states and allow for a mapping of the PESs of the core-excited molecules [71].

### C. Angular distribution of RA electrons

The angular anisotropy parameters of the emitted electrons were extracted from the spectra of Fig. 3 by using the conventional formula $\beta^e = 2(I_{0^\circ} - I_{90^\circ})/(I_{0^\circ} + 2I_{90^\circ})$. In order to extract $\beta^e$ parameters for individual final vibronic states, a peak fitting procedure was applied to the electron spectra using the SPANCF macros for Igor Pro (Wavemetrics, Inc.) developed by Kukk [72,73]. As discussed in the preceding section, not all vibronic states, clearly seen in the overview spectrum in Fig. 2, can always be resolved, especially on the low-energy side of the resonance. Also, it was not always possible to disentangle overlapping vibronic states. We thus focused our analysis on those states where vibrationally resolved $\beta^e$ parameters can unambiguously be determined at each photon energy.

In the present fitting procedure, the peak positions and widths were determined using the spectrum recorded off resonance [Fig. 3(a)], and only the intensity of the vibrational sublevels was a free parameter. The vibrational spacings found for the off-resonance ionization were similar to those reported earlier [53]. The present fitting includes two symmetric stretching vibrational progressions $X(\nu_1\nu_2 0)$ for the bending

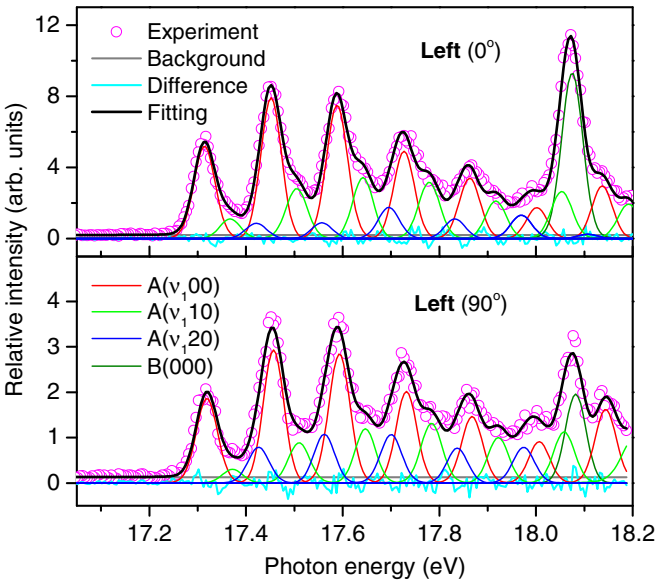


FIG. 4. (Color online) Typical results of the fitting procedure used to disentangle overlapping vibronic states. The experimental spectra (open circles) were obtained at the photon energy of 290.37 eV (corresponds to the vertical arrow labeled "Left" in Fig. 1). The binding energy range with a dominant contribution from the overlapping $A\,^2\Pi_u$ and $B\,^2\Sigma_u^+$ states is shown for the electrons detected parallel (0°, top panel) and perpendicular (90°, bottom panel) to the polarization vector of the x-ray photons. The fitting procedure includes constant background and the $A\,^2\Pi_u(\nu_1\nu_2 0)$ and $B\,^2\Sigma_u^+(000)$ vibronic states (see legend). The difference residual between the measured and fitted total spectra is also shown for completeness.

quanta $\nu_2 = 0,1$, three symmetric stretching progressions $A(\nu_1\nu_2 0)$ corresponding to the bending quanta $\nu_2 = 0,1,2$, and only the vibrational ground states $B(000)$ and $C(000)$. A typical outcome of the peak fitting is shown in Fig. 4 for a selected binding energy range and photon energy (see caption for details). The present experimental $\beta^e$ parameters obtained for individual final vibronic states are collected in Table I. The error bars for the $\beta$ parameters were estimated via Eq. (2) from Ref. [47].

In the off-resonance ionization regime (second column of Tab. I), the vibrational progressions of $X$ and $A$ states exhibit similar $\beta^e$ values for all resolved vibrational levels ($\beta_X^e \sim 1.48$ and $\beta_A^e \sim 1.35$). This is in accordance with the expectation that the angular distributions should not change between vibrational levels in the absence of non-Franck-Condon effects [74], multichannel interferences [28–33], or shape resonances [75,76]. In the on-resonance excitation, however, significant changes in the angular distribution parameters can be expected, and these changes are usually much stronger than for the total RA electron intensities [77,78]. From Table I it is evident that the $\beta^e$ values recorded on-resonance (columns 4, 6, and 8) are systematically smaller than the off-resonance values (second column), which implies a dip in the energy dependence of $\beta^e(\omega)$.

Figure 5 summarizes the computed energy dependencies of the angular distribution parameters $\beta^e(\omega)$ for the selected individual final vibronic states. For comparison, the available experimental data from Table I are also depicted in this figure,

TABLE I. Vibrationally resolved angular distribution parameters $\beta^e$ measured and computed in the present work for different final RA decay states at different excitation energies in the vicinity of the C $1s \rightarrow \pi^*$ resonance of $CO_2$. The experimental uncertainties are given in parentheses as $1.48(1) \equiv 1.48 \pm 0.01$.

| | Off-resonance (285 eV) | | Left (290.37 eV) | | Top (290.77 eV) | | Right (291.17 eV) | |
|---|---|---|---|---|---|---|---|---|
| State | Experiment | Theory | Experiment | Theory | Experiment | Theory | Experiment | Theory |
| $X(000)$ | 1.48(1) | 1.23 | 1.30(2) | 1.21 | 1.44(1) | 1.26 | 1.42(2) | 1.27 |
| $X(100)$ | 1.49(2) | 1.23 | 1.29(4) | 1.18 | 1.07(2) | 1.19 | 1.36(3) | 1.28 |
| $A(000)$ | 1.33(6) | 1.08 | 0.75(2) | 0.80 | 0.68(5) | 0.98 | 1.21(6) | 1.03 |
| $A(100)$ | 1.37(3) | 1.08 | 0.74(2) | 0.72 | 0.71(5) | 0.89 | 1.08(3) | 0.99 |
| $A(200)$ | 1.34(3) | 1.08 | 0.72(2) | 0.65 | 0.73(5) | 0.81 | 1.10(3) | 0.93 |
| $A(300)$ | 1.34(3) | 1.08 | 0.66(3) | 0.66 | 0.70(5) | 0.73 | 1.06(2) | 0.86 |
| $A(400)$ | 1.39(3) | 1.08 | 0.63(6) | 0.65 | 0.56(7) | 0.66 | 0.85(2) | 0.79 |
| $A(500)$ | 1.40(5) | 1.08 | 0.46(5) | 0.64 | 0.48(9) | 0.57 | 0.73(1) | 0.72 |
| $A(600)$ | 1.26(7) | 1.08 | 0.41(9) | 0.64 | 0.72(10) | 0.62 | 0.62(1) | 0.68 |
| $B(000)$ | 1.54(10) | 1.38 | 1.10(5) | 0.97 | 0.86(10) | 0.90 | 1.10(11) | 1.00 |
| $C(000)$ | 1.71(1) | 1.56 | 1.67(2) | 1.50 | 1.67(2) | 1.42 | 1.74(2) | 1.47 |

and the $\beta^e$ values computed at four selected excitation energies are listed in the columns 3, 5, 7, and 9 of Table I. The figure and the table illustrate a good overall agreement between the computed and the measured anisotropy parameters. Qualitatively, the present calculations support a window-type resonant

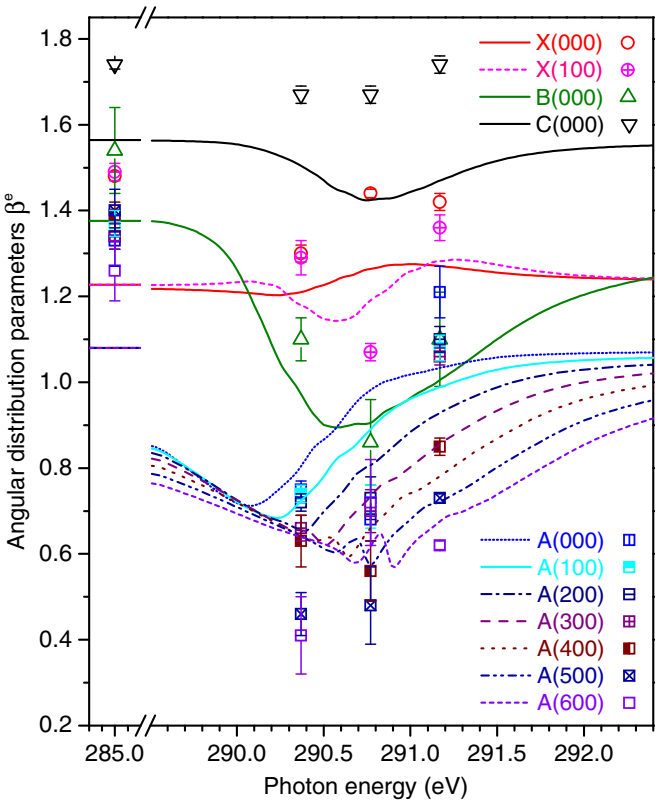


FIG. 5. (Color online) The theoretical (depicted by lines) angular distribution parameters $\beta^e$ of the RA electrons computed in the present work for selected vibrational states ($\nu_1 00$) of the $X$, $A$, $B$, and $C$ participator decay channels (see legends) as functions of the photon energy in the vicinity of the C $1s \rightarrow \pi^*$ resonance of $CO_2$. The energy-axis break on the left-hand side is introduced to visually separate data for the off- and on-resonance excitation regimes. The experimental data (depicted by symbols) are those listed in Table I.

dependence of the $\beta^e(\omega)$ profiles suggested above. In addition, similar individual trends in the energy dependence of the computed and measured $\beta^e(\omega)$ profiles are seen from Fig. 5. Quantitatively, our computed $\beta^e(\omega)$ values are systematically (by about 0.2) lower than the measured values.

In spite of a very small influence of the resonant channel on the intensity envelope of the $CO_2^+(X)$ state, the $\beta^e(\omega)$ for $X(000)$ and $X(100)$ substates change considerably across the resonance. The computed and measured energy dependencies show similar sign of interference effects, but the computed variations are somewhat weaker. The two states exhibit different energy variations, which can be associated with the sign-reversal behavior of the Franck-Condon factors for RA decay. The effect of the interference on the computed and measured angular distribution of the $C(000)$ electrons is similar. For the $B(000)$ state, the interference introduces a broad and steep dip in the energy dependence of the $\beta^e(\omega)$ parameter. The computed and measured depths of the energy profile are very similar but the computed profile is somewhat broader.

For the $A(\nu_1 00)$ states, the experimental and theoretical $\beta^e(\omega)$ parameters exhibit qualitatively similar profiles for different $\nu_1$ levels, i.e., slow and broad decrease on the low-energy side of the resonance, and somewhat steeper increase on the high-energy side. Quantitatively, these dependencies are different for different $\nu_1$ levels. This can be associated with the impact of ESI between the direct and resonance ionization amplitudes. For higher $\nu_1$ levels, the relative contribution of the direct ionization channel decreases compared to the resonant one. The latter channel thus extends its influence to larger energy detunings, which results in broader profiles for higher $\nu_1$ levels. Finally, slight wiggling in the computed $\beta^e(\omega)$ profiles in the middle of the resonance can be associated with the effect of LVI.

## V. CONCLUSIONS

We studied the excitation and the RA decay of the $CO_2$ molecule at different photon energies along the C $1s \rightarrow \pi^*$ resonance, both experimentally and theoretically. In the experiment, the electron spectra due to the participator Auger decay into the $X$, $A$, $B$, and $C$ final $CO_2^+$ ionic states were

recorded with vibrational and angular resolutions and a narrow bandwidth for the excitation. This allowed determination of the individual angular distribution parameters $\beta^e$ for several final vibronic states. In the theory, the differential cross sections for the photoionization of $CO_2$ were calculated in the broad energy range across the C $1s \rightarrow \pi^*$ resonance. The electronic properties of the molecular photoionization process were computed by the SC method, and the nuclear dynamics by the MCTDH method. The computed RA electron intensities and angular distribution parameters are found in good overall agreement with the measured ones.

We found significant changes of the RA electron intensity distribution as functions of the excitation energy and final vibronic states. Those changes were also observed in the previous, lower resolutions experiments on $C^*O_2$ [21,67] and attributed to the excitation and decay of different vibrational states of the two overlapping resonances with bent $^1A_1$ and linear $^1B_1$ geometry. Here we observed that the electron angular distribution parameters exhibit even stronger changes across the resonance and with respect to the final-state vibrational envelope. The off- and on-resonance measurements at four selected photon energies suggest a dip in the energy dependence of $\beta^e(\omega)$ parameters of the $X$, $A$, $B$, and $C$ states.

The present calculations attribute those observations to a complex interplay of the following main effects. The first effect is ESI between the direct and resonant ionization pathways, which induces a broad energy dependence of the angular distribution parameters [77,78]. The second one is the ESI between the intermediate bent $^1A_1$ and the linear $^1B_1$ electronic resonances, which is symmetry forbidden in the total spectra but is allowed in the angularly resolved ones [31,32]. The third is the LVI, since the natural width of the electronic resonance 95 meV [64] is comparable with the energy spacings between the symmetric stretching and bending levels (equal to about 156 and 102 meV, respectively [21]). The relative importance of these effects changes across the resonance and final-state vibrational envelope. Finally, other types of interference relevant to polyatomics [30] may also play a role in $C^*O_2$.

Polyatomic molecules, where several relevant degrees of freedom can contribute to nuclear dynamics, are an interesting class of targets for angularly resolved RA electron spectroscopy. The increased complexity of the process, however, makes detailed theoretical interpretation of the observed effects challenging. In order to perform a more accurate quantitative analysis of the individual impact of different interference mechanisms involved in the RA decay of $C^*O_2$, several improvements of the present theory need to be performed. First of all, the fixed nuclei approximation has to be lifted, and the geometry-dependent electronic transition amplitudes need to be incorporated in the underlying nuclear dynamics calculations. In addition, the final-state continuum channel coupling may play a role as well in the present case. Experimentally, the quasicontinuous measurement of the energy-dependence of the $\beta^e$ parameters along the resonance profile will also provide deeper insight into our understanding of the process.

## ACKNOWLEDGMENTS

The experiments were performed at the PLEIADES beamline at the SOLEIL Synchrotron, France. We thank E. Robert for technical assistance and the SOLEIL staff for stable operation of the equipment and storage ring during the experiments. We acknowledge F. Gel'mukhanov and N. Kosugi for fruitful discussions. The European COST action CM1204XUV/X-ray light and fast ions for ultrafast chemistry (XLIC) is acknowledged. This work was partly supported by State Hessen Initiative for the Development of Scientific and Economic Excellence (LOEWE) within the focus project Electron Dynamics of Chiral Systems (ELCH). Financial support by the Deutsche Forschungsgemeinschaft (DFG Project No. DE 2366/1-1) and by the Southern Federal University within inner Project No. 213.01.-07.2014/11PPIG is gratefully acknowledged. V.L.S. would like to thank the Institute of Physics, University of Kassel, for the hospitality during his stay there.

[1] G. S. Brown, M. H. Chen, B. Crasemann, and G. E. Ice, Phys. Rev. Lett. **45**, 1937 (1980).

[2] A. Kivimäki, A. Naves de Brito, S. Aksela, H. Aksela, O.-P. Sairanen, A. Ausmees, S. J. Osborne, L. B. Dantas, and S. Svensson, Phys. Rev. Lett. **71**, 4307 (1993).

[3] F. Gel'mukhanov and H. Ågren, Phys. Rep. **312**, 87 (1999).

[4] C. Miron and P. Morin, in *Handbook of High-resolution Spectroscopy*, edited by M. Quack and F. Merkt (Wiley & Sons, Chichester, UK, 2011).

[5] M. N. Piancastelli, R. F. Fink, R. Feifel, M. Bssler, S. L. Sorensen, C. Miron, H. Wang, I. Hjelte, O. Bjrneholm, A. Ausmees, S. Svensson, P. Salek, F. K. Gel'mukhanov, and H. Ågren, J. Phys B **33**, 1819 (2000).

[6] A. Ehresmann, L. Werner, S. Klumpp, S. Lucht, H. Schmoranzer, S. Mickat, R. Schill, K. H. Schartner, Ph. V. Demekhin, M. P. Lemeshko, and V. L. Sukhorukov, J. Phys. B **39**, 283 (2006).

[7] C. Miron, C. Nicolas, O. Travnikova, P. Morin, Y. Sun, F. Gel'mukhanov, N. Kosugi, and V. Kimberg, Nat. Phys. **8**, 135 (2012).

[8] V. Kimberg, A. Lindblad, J. Söderström, O. Travnikova, C. Nicolas, Y. P. Sun, F. Gel'mukhanov, N. Kosugi, and C. Miron, Phys. Rev. X **3**, 011017 (2013).

[9] M. Neeb, J.-E. Rubensson, M. Biermann, and W. Eberhardt, J. Electron Spectrosc. Relat. Phenom. **67**, 261 (1994).

[10] S. L. Sorensen, R. Fink, R. Feifel, M. N. Piancastelli, M. Bässler, C. Miron, H. Wang, I. Hjelte, O. Björneholm, and S. Svensson, Phys. Rev. A **64**, 012719 (2001).

[11] T. X. Carroll, M. Coville, P. Morin, and T. D. Thomas, J. Chem. Phys. **101**, 998 (1994).

[12] E. Kukk, G. Snell, J. D. Bozek, W.-T. Cheng, and N. Berrah, Phys. Rev. A **63**, 062702 (2001).

[13] H. Wang, R. F. Fink, M. N. Piancastelli, I. Hjelte, K. Wiesner, M. Bässler, R. Feifel, O. Björneholm, C. Miron, A. Giertz,

F. Burmeister, S. L. Sorensen, and S. Svensson, J. Phys. B **34**, 4417 (2001).
[14] A. Ehresmann, W. Kielich, L. Werner, Ph. V. Demekhin, D. V. Omel'yanenko, V. L. Sukhorukov, K. H. Schartner, and H. Schmoranzer, Eur. Phys. J. D **45**, 235 (2007).
[15] M. Patanen, S. Urpelainen, M. Huttula, R. Sankari, V. Kisand, E. Nommiste, E. Kukk, H. Aksela, and S. Aksela, Phys. Rev. A **80**, 013414 (2009).
[16] J.-C. Liu, C. Nicolas, Y.-P. Sun, R. Flammini, P. O'Keefe, L. Avaldi, P. Morin, V. Kimberg, N. Kosugi, F. Gel'mukhanov, and C. Miron, J. Phys. Chem. B **115**, 5103 (2011).
[17] O. Travnikova, V. Kimberg, R. Flammini, X.-J. Liu, P. Patanen, C. Nicolas, S. Svensson, and C. Miron, J. Phys. Chem. Lett. **4**, 2361 (2013).
[18] K. Ueda, M. Okunishi, H. Chiba, Y. Shimizu, K. Ohmori, Y. Sato, E. Shigemasa, and N. Kosugi, Chem. Phys. Lett. **236**, 311 (1995).
[19] A. Kivimäkiy, M. Neeb, B. Kempgens, H. M. Köppe, and A. M. Bradshaw, J. Phys. B **29**, 2701 (1996).
[20] C. Miron, P. Morin, D. Céolin, L. Journel, and M. Simon, J. Chem. Phys. **128**, 154314 (2008).
[21] E. Kukk, J. D. Bozek, and N. Berrah, Phys. Rev. A **62**, 032708 (2000).
[22] C. Miron, M. Simon, P. Morin, S. Nanbu, N. Kosugi, S. L. Sorensen, A. Naves de Brito, M. N. Piancastelli, O. Björnehom, R. Feifel, M. Bässler, and S. Svensson, J. Chem. Phys. **115**, 864 (2001).
[23] M. N. Piancastelli, D. Céolin, O. Travnikova, Z. Bao, M. Hoshino, T. Tanaka, H. Kato, H. Tanaka, J. R. Harries, Y. Tamenori, G. Prümper, T. Lischke, X. J. Liu, and K. Ueda, J. Phys. B **40**, 3357 (2007).
[24] O. Travnikova, C. Miron, M. Bässler, R. Feifel, M. N. Piancastelli, S. L. Sorensen, and S. Svensson, J. Electron Spectrosc. Relat. Phenom. **174**, 100 (2009).
[25] P. Morin, M. Simon, C. Miron, N. Leclercq, and D. L. Hansen, J. Electron Spectrosc. Relat. Phenom. **93**, 49 (1998).
[26] C. Miron and P. Morin, Nucl. Instrum. Methods Phys. Res. Sect. A **601**, 66 (2009).
[27] V. Schmidt, Rep. Prog. Phys. **55**, 1483 (1992).
[28] Ph. V. Demekhin, I. D. Petrov, V. L. Sukhorukov, W. Kielich, P. Reiss, R. Hentges, I. Haar, H. Schmoranzer, and A. Ehresmann, Phys. Rev. A **80**, 063425 (2009); Erratum: **81**, 069902(E) (2010).
[29] Ph. V. Demekhin, I. D. Petrov, T. Tanaka, M. Hoshino, H. Tanaka, K. Ueda, W. Kielich, and A. Ehresmann, J. Phys. B **43**, 065102 (2010).
[30] C. Miron, V. Kimberg, P. Morin, C. Nicolas, N. Kosugi, S. Gavrilyuk, and F. Gel'mukhanov, Phys. Rev. Lett. **105**, 093002 (2010).
[31] Ph. V. Demekhin, I. D. Petrov, V. L. Sukhorukov, W. Kielich, A. Knie, H. Schmoranzer, and A. Ehresmann, Phys. Rev. Lett. **104**, 243001 (2010).
[32] Ph. V. Demekhin, I. D. Petrov, V. L. Sukhorukov, W. Kielich, A. Knie, H. Schmoranzer, and A. Ehresmann, J. Phys. B **43**, 165103 (2010).
[33] A. Lindblad, V. Kimberg, J. Söderström, C. Nicolas, O. Travnikova, N. Kosugi, F. Gel'mukhanov, and C. Miron, New J. Phys. **14**, 113018 (2012).
[34] E. Kukk, J. D. Bozek, W.-T. Cheng, R. F. Fink, A. A. Wills, and N. Berrah, J. Chem. Phys. **111**, 9642 (1999).
[35] O. Hemmers, F. Heiser, J. Viefhaus, K. Wieliczek, and U. Becker, J. Phys. B **32**, 3769 (1999).
[36] H. Wang, R. F. Fink, M. N. Piancastelli, M. Bässler, I. Hjelte, O. Björneholm, F. Burmeister, R. Feifel, A. Giertz, C. Miron, S. L. Sorensen, K. Wiesner, and S. Svensson, Chem. Phys. **289**, 31 (2003).
[37] Y. Shimizu, H. Ohashi, Y. Tamenori, Y. Muramatsu, H. Yoshida, K. Okada, N. Saito, H. Tanaka, I. Koyano, S. Shin, and K. Ueda, J. Electron Spectrosc. Relat. Phenom. **114–116**, 63 (2001).
[38] I. Hjelte, L. Karlsson, S. Svensson, A. De Fanis, V. Carravetta, N. Saito, M. Kitajima, H. Tanaka, H. Yoshida, A. Hiraya, I. Koyano, K. Ueda, and M. N. Piancastelli, J. Chem. Phys. **122**, 084306 (2005).
[39] A. Knie, M. Ilchen, Ph. Schmidt, Ph. Reiß, C. Ozga, B. Kambs, A. Hans, N. Muglich, S. A. Galitskiy, L. Glaser, P. Walter, J. Viefhaus, A. Ehresmann, and Ph. V. Demekhin, Phys. Rev. A **90**, 013416 (2014).
[40] Y. Muramatsu, K. Ueda, N. Saito, H. Chiba, M. Lavollée, A. Czasch, T. Weber, O. Jagutzki, H. Schmidt-Böcking, R. Moshammer, U. Becker, K. Kubozuka, and I. Koyano, Phys. Rev. Lett. **88**, 133002 (2002).
[41] J. Adachi, N. Kosugi, E. Shigamasa, and A. Yagashita, J. Chem. Phys. **107**, 4919 (1997).
[42] J. Adachi, N. Kosugi, E. Shigemasa, and A. Yagishita, J. Chem. Phys. **102**, 7369 (1995).
[43] J. Adachi, N. Kosugi, E. Shigamasa, and A. Yagashita, J. Phys. Chem. **100**, 19783 (1996).
[44] J. Söderström, A. Lindblad, A. Grum-Grzhimailo, O. Travnikova, N. Nicolas, S. Svensson, and C. Miron, New J. Phys. **13**, 073014 (2011).
[45] O. Travnikova, J. C. Liu, A. Lindblad, C. Nicolas, J. Söderström, V. Kimberg, F. Gel'mukhanov, and C. Miron, Phys. Rev. Lett. **105**, 233001 (2010).
[46] A. R. Milosavljević, F. Canon, C. Nicolas, C. Miron, L. Nahon, and A. Giuliani, J. Phys. Chem. Lett. **3**, 1191 (2012).
[47] M. Patanen, O. Travnikova, M. G. Zahl, J. Söderström, P. Decleva, T. D. Thomas, S. Svensson, N. Mårtensson, K. J. Børve, L. J. Saethre, and C. Miron, Phys. Rev. A **87**, 063420 (2013).
[48] O. Sublemontier, C. Nicolas, D. Aureau, M. Patanen, H. Kintz, X. Liu, M.-A. Gaveau, J.-L. Le Garrec, E. Robert, F.-A. Barreda, A. Etcheberry, C. Reynaud, J. B. Mitchell, and C. Miron, J. Phys. Chem. Lett. **5**, 3399 (2014).
[49] E. Antonsson, M. Patanen, C. Nicolas, J. J. Neville, S. Benkoula, A. Goel, and C. Miron, Phys. Rev. X **5**, 011025 (2015).
[50] P. Baltzer, L. Karlsson, M. Lundqvist, and B. Wannberg, Rev. Sci. Instrum. **64**, 2179 (1993).
[51] T. D. Thomas, E. Kukk, K. Ueda, T. Ouchi, K. Sakai, T. X. Carroll, C. Nicolas, O. Travnikova, and C. Miron, Phys. Rev. Lett. **106**, 193009 (2011).
[52] Q. Miao, O. Travnikova, F. Gel'mukhanov, V. Kimberg, Y.-P. Sun, T. D. Thomas, C. Nicolas, M. Patanen, and C. Miron, J. Phys. Chem. Lett. **6**, 1568 (2015).
[53] P. Baltzer, F. T. Chau, J. H. D. Eland, L. Karlsson, M. Lundquist, J. Rostas, K. Y. Tam, H. Veenhuizen, and B. Wannberg, J. Chem. Phys. **104**, 8922 (1996).
[54] H.-D. Meyer, U. Manthe, and L. S. Cederbaum, Chem. Phys. Lett. **165**, 73 (1990).
[55] G. A. Worth, M. H. Beck, A. Jäckle, and H.-D. Meyer, *The Multiconfiguration Time-Dependent Hartree (MCTDH) Package*; see http://www.pci.uni-heidelberg.de/cms/mctdh.html

[56] A. Ehresmann, H. Liebel, H. Schmoranzer, B. Zimmermann, S. Kammer, K.-H. Schartner, Ph. V. Demekhin, and V. L. Sukhorukov, J. Phys. B **36**, 3669 (2003).
[57] A. Ehresmann, L. Werner, S. Klumpp, H. Schmoranzer, Ph. V. Demekhin, B. M. Lagutin, V. L. Sukhorukov, S. Mickat, S. Kammer, B. Zimmermann, and K.-H. Schartner, J. Phys. B **37**, 4405 (2004).
[58] Ph. V. Demekhin, D. V. Omel'yanenko, B. M. Lagutin, V. L. Sukhorukov, L. Werner, A. Ehresmann, K.-H. Schartner, and H. Schmoranzer, Opt. Spectrosc. **102**, 318 (2007).
[59] Ph. V. Demekhin, V. L. Sukhorukov, and A. Ehresmann, J. Chem. Phys. **134**, 024113 (2011).
[60] S. A. Galitskiy, A. N. Artemyev, K. Jänkälä, B. M. Lagutin, and Ph. V. Demekhin, J. Chem. Phys. **142**, 034306 (2015).
[61] A. N. Artemyev, A. D. Müller, D. Hochstuhl, and Ph. V. Demekhin, J. Chem. Phys. **142**, 244105 (2015).
[62] F. K. Gel'mukhanov, L. N. Mazalov, and A. V. Kondratenko, Chem. Phys. Lett. **46**, 133 (1977).
[63] A. Cesar and H. Ågren, Phys. Rev. A **45**, 2833 (1992).
[64] T. Hatamoto, M. Matsumoto, X.-J. Liu, K. Ueda, M. Hoshino, N. Nakagawa, T. Tanaka, H. Tanaka, M. Ehara, R. Tamaki, and H. Nakatsuji, J. Electron Spectrosc. Relat. Phenom. **155**, 54 (2007).
[65] M. N. Piancastelli, A. Kivimäki, B. Kempgens, M. Neeb, K. Maier, and A. M. Bradshaw, Chem. Phys. Lett. **274**, 13 (1997).
[66] K. Lee, D. Y. Kim, C. I. Ma, and D. M. Hanson, J. Chem. Phys. **100**, 8550 (1994).
[67] P. Morin, M. Simon, C. Miron, N. Leclercq, E. Kukk, J. D. Bozek, and N. Berrah, Phys. Rev. A **61**, 050701(R) (2000).
[68] D. Céolin, C. Miron, M. Simon, and P. Morin, J. Electron Spectrosc. Relat. Phenom. **141**, 171 (2004).
[69] M. Th. Praet, J. C. Lorquet, and G. Raseev, J. Chem. Phys. **77**, 4611 (1982).
[70] R. Polak, M. Hochlaf, M. Levinas, G. Chambaud, and P. Rosmus, Spectrochim. Acta A **55**, 447 (1999).
[71] C. Miron, R. Feifel, O. Björnehom, S. Svensson, A. Naves de Brito, S. L. Sorensen, M. N. Piancastelli, M. Simon, and P. Morin, Chem. Phys. Lett. **359**, 48 (2002).
[72] E. Kukk, SPANCF, Spectral Analysis by Curve Fitting Macro Package.
[73] E. Kukk, K. Ueda, U. Hergenhahn, X.-J. Liu, G. Prümper, H. Yoshida, Y. Tamenori, C. Makochekanwa, T. Tanaka, M. Kitajima, and H. Tanaka, Phys. Rev. Lett. **95**, 133001 (2005).
[74] A. C. Parr, D. L. Ederer, J. B. West, D. M. P. Holland, and J. L. Dehmer, J. Chem. Phys. **76**, 4349 (1982).
[75] R. R. Lucchese, J. Söderström, T. Tanaka, M. Hoshino, M. Kitajima, H. Tanaka, A. De Fanis, J.-E. Rubensson, and K. Ueda, Phys. Rev. A **76**, 012506 (2007).
[76] M. Hoshino, K. Nakagawa, T. Tanaka, M. Kitajima, H. Tanaka, A. De Fanis, K. Wang, B. Zimmermann, V. McKoy, and K. Ueda, J. Phys. B **39**, 3047 (2006).
[77] B. M. Lagutin, I. D. Petrov, V. L. Sukhorukov, S. Kammer, S. Mickat, R. Schill, K.-H. Schartner, A. Ehresmann, Y. A. Shutov, and H. Schmoranzer, Phys. Rev. Lett. **90**, 073001 (2003).
[78] B. M. Lagutin, I. D. Petrov, V. L. Sukhorukov, Ph. V. Demekhin, B. Zimmermann, S. Mickat, S. Kammer, K.-H. Schartner, A. Ehresmann, Y. A. Shutov, and H. Schmoranzer, J. Phys. B **36**, 3251 (2003).